Published by Institute of Physics Publishing for SISSA

Received: *April 6, 2006*
Revised: *June 20, 2006*
Accepted: *July 16, 2006*
Published: *August 17, 2006*

Leptonic charged Higgs decays in the Zee model

Diego Aristizabal Sierra

AHEP Group, Instituto de Física Corpuscular – C.S.I.C./Universitat de València
Edificio de Institutos de Paterna
Apartado 22085, E–46071 València, Spain
E-mail: daristi@ific.uv.es

Diego Restrepo

Instituto de Física, Universidad de Antioquia
A.A. 1226 Medellín, Colombia
E-mail: restrepo@uv.es

Abstract: We consider the version of the Zee model where both Higgs doublets couple to leptons. Within this framework we study charged Higgs decays. We focus on a model with minimal number of parameters consistent with experimental neutrino data. Using constraints from neutrino physics we (i) discuss the reconstruction of the parameter space of the model using the leptonic decay patterns of both of the two charged Higgses, $h^+_{1,2} \to \ell^+_j \nu_i$, and the decay of the heavier charged Higgs, $h^+_2 \to h^+_1 h^0$; (ii) show that the decay rate $\Gamma(h^+_1 \to \mu^+\nu_i)$ in general is enhanced in comparision to the standard two Higgs doublet model while in some regions of parameter space $\Gamma(h^+_1 \to \mu^+\nu_i)$ even dominates over $\Gamma(h^+_1 \to \tau^+\nu_i)$.

Keywords: Beyond Standard Model, Neutrino Physics, Higgs Physics.

Contents

1. Introduction

Neutrino oscillation experiments, including the results of KamLAND [1] have confirmed the LMA-MSW oscillation solution of the solar neutrino problem. Together with the earlier discoveries in atmospheric neutrinos [2], one can be fairly confident that all neutrino flavours mix and that at least two non-zero neutrino masses exist.

In the standard model neutrinos are massless. Among all the existing models to generate small neutrino Majorana masses the seesaw mechanism [3] is perhaps the most popular. However, this is not the only theoretical approach to neutrino masses. Other possibilities include Higgs triplets [4], supersymmetric models with broken R-parity [5, 6], some hybrid mechanisms that combine the triplet and the R-parity ideas [7] and radiative mechanisms [8, 9].

Here we consider a particular radiative mechanism, the Zee model [8]. In this model the scalar sector of the standard model is enlarged to include a charged SU(2) gauge singlet scalar and a second Higgs doublet. This particle content allows to write an explicit lepton number (L) violating term in the scalar potential and leads to neutrino masses at one loop order. In the Minimal Zee Model (MZM), only one Higgs doublet couples to leptons [10]. As a result, dangerous Flavour Changing Neutral Current (FCNC) processes are forbidden. It has been shown [11] that combining SNO, KamLAND and K2K experimental data this version is ruled out.

However, this does not mean that the Zee model is ruled out. The original version, from now on called the General Zee Model (GZM) [12], in which both of the two Higgs doublets couple to the matter fields has been shown [11 − 13] to be consistent with atmospheric and solar neutrino data as well [14].

Once one allows both of the Higgs doublets to couple to leptons the number of model parameters increases. Here instead of working with all the couplings of the model we will consider a scheme, previously discussed in references [12, 13], where the neutrino mass matrix has a two-zero-texture. This particular GZM will be called Next to MZM (NMZM).

In the Higgs sector, after spontaneous breaking of the electroweak symmetry, the charged gauge singlet mixes with the charged components of the two Higgs doublets. The resulting charged Higgs eigenstates ($h_i^{\pm}$ with $i = 1, 2$) decay to states with charged leptons and neutrinos. These decays can be used, in principle, to reconstruct the Majorana neutrino mass matrix.

We will show that due to the constraints imposed by neutrino physics, the $Br(h_1^+ \to \sum_i \nu_i \mu^+)$ is enhanced in comparision to the two-Higgs doublet models (2HDM) of type-I and type-II [1]. Moreover, we will show that in large parts of the parameter space $Br(h_1^+ \to \sum_i \nu_i \mu^+) \gtrsim Br(h_1^+ \to \sum_i \nu_i \tau^+)$. For details see section 6.

The rest of this paper is organized as follows. In section 2 we give the generalities of the GZM and work out the Higgs mass spectrum of the model. In section 3 we study charged Higgs production at a future e^+e^- collider. In section 4 we discuss the bounds on the parameters of the model coming from FCNC processes constraints. In section 5 we describe the Majorana neutrino mass matrix within the GZM and in the NMZM. In section 6 we discuss the connection between neutrino physics and charged Higgs decays. In section 7 we present our conclusions and summarize our results.

2. The model

2.1 Generalities

If no new fermions are added to the standard model neutrino masses must be always of Majorana type, i.e. the mass term must violate L. In the Zee model an $L = 2$ charged scalar, h^+, is introduced. Since this field carries electric charge its vacumm expectation value (vev) must vanish. Therefore in this model L cannot be spontaneously broken.

[1] In type-I only one of the Higgs fields couples to the SM fermions, in type-II one Higgs field couples to up-type quarks and the other Higgs field couples to down-type quarks. There is another version called type-III [15] where both Higgs fields couple to all SM fermions.

However, h^+ can be used to drive the lepton number breaking from the leptonic sector to the scalar sector. In order to accomplish this a new $\mathrm{SU}(2)_L$ doublet has to be added, as a result an explicit L violation term can be written. This term is given by

$$\mu \epsilon_{\alpha\beta} \Phi_1^\alpha \Phi_2^\beta h^- + \mathrm{H.c.} \tag{2.1}$$

where μ is a coupling with dimension of mass and Φ_1 and Φ_2 are doublets with hypercharge $Y_1 = Y_2 = 1$.

The most general Yukawa couplings of the model can be written as

$$-\mathcal{L}_Y = \bar{L}_i (\Pi_a)_{ij} \Phi_a e_{Rj} + \epsilon_{\alpha\beta} \bar{L}_i^\alpha f_{ij}\, C(\bar{L}^T)_j^\beta h^- + \mathrm{H.c.}\,, \tag{2.2}$$

where L_i are lepton doublets, e_{Rj} are lepton singlets, C is the charge conjugation operator, Π_a $(a = 1, 2)$ and f are 3×3 matrices in flavour space, $\epsilon_{\alpha\beta}$ $(\alpha, \beta = 1, 2)$ is the $\mathrm{SU}(2)_L$ antisymmetric tensor and $i, j = 1, 2, 3$ are family indices. f is an antisymmetric matrix due to Fermi statistics.

In general both of the two Higgs doublets can acquire vev's, $\langle \Phi_a \rangle = v_a$, with $v = \sqrt{v_1^2 + v_2^2} \simeq 246\,\mathrm{GeV}$. As usual, the ratio of these vev's can be parametrized as $\tan\beta = v_2/v_1$.

2.2 Higgs potential and scalar mass spectrum

Though in this work we are interested mainly in the charged Higgs sector of the model and its relation with neutrino physics, we will briefly discuss the full scalar mass spectrum.

Assuming that the Higgs Potential is CP-conserving, in the most general 2HDM SO(2) transformations between the two Higgs fields

$$\begin{pmatrix} H_1 \\ H_2 \end{pmatrix} = \begin{pmatrix} \cos\beta & \sin\beta \\ -\sin\beta & \cos\beta \end{pmatrix} \begin{pmatrix} \Phi_1 \\ \Phi_2 \end{pmatrix}, \tag{2.3}$$

and between the two Yukawa matrices in eq. (2.2)

$$\begin{pmatrix} \Pi_1' \\ \Pi_2' \end{pmatrix} = \begin{pmatrix} \cos\beta & \sin\beta \\ -\sin\beta & \cos\beta \end{pmatrix} \begin{pmatrix} \Pi_1 \\ \Pi_2 \end{pmatrix}, \tag{2.4}$$

do not change the functional form of the Lagrangian. In particular, there is no distinction between the two complex hypercharge-one SO(2) doublet scalar fields, Φ_a. Thus, any two orthonormal linear combinations of these two fields can serve as a basis for the Lagrangian. Since the definition of $\tan\beta$ assumes that one can distinguish between the two identical hypercharge-one Higgs doublet fields, clearly, $\tan\beta$ is a basis-dependent quantity, and hence is not a physical parameter [16, 17]. This parameter disappears completely if one transforms to the Higgs basis in which only one of the two Higgs doublets acquire a vev. This suggest that the Higgs basis is special. In fact, the Lagrangian parameters with respect to the Higgs basis are related to physical parameters which can be written in terms of quantities that are invariant under arbitrary basis transformations in the space of fields. In this way, in the Higgs basis one can readily identify the relevant invariant quantities involved in the determination of the physical masses. In eq. (2.4), Π_1' and Π_2' are invariant quantities [16]. They coincide with the Lagrangian parameters in the Higgs basis.

JHEP08(2006)036

In the Higgs basis the most general gauge invariant scalar potential of the model, consistent with renormalizability reads

$$
\begin{aligned}
V =\; & \mu_1^2 H_1^\dagger H_1 + \mu_2^2 H_2^\dagger H_2 - [\mu_3^2 H_1^\dagger H_2 + \text{H.c.}] + \frac{1}{2}\lambda_1 (H_1^\dagger H_1)^2 \\
& + \frac{1}{2}\lambda_2 (H_2^\dagger H_2)^2 + \lambda_3 (H_1^\dagger H_1)(H_2^\dagger H_2) + \lambda_4 (H_1^\dagger H_2)(H_2^\dagger H_1) \\
& + \left\{ \frac{1}{2}\lambda_5 (H_1^\dagger H_2)^2 + [\lambda_6 (H_1^\dagger H_1) + \lambda_7 (H_2^\dagger H_2)] H_1^\dagger H_2 + \text{H.c.} \right\} \\
& + \mu_h^2 |h^+|^2 + \lambda_h |h^+|^4 + \lambda_8 |h^+|^2 H_1^\dagger H_1 + \lambda_9 |h^+|^2 H_2^\dagger H_2 \\
& + \lambda_{10} |h^+|^2 (H_1^\dagger H_2 + \text{H.c.}) + \mu \epsilon_{\alpha\beta} H_1^\alpha H_2^\beta h^- .
\end{aligned}
\tag{2.5}
$$

Since we will not deal with CP-violating effects we only consider real coefficients. The SO(2)-invariants of the Higgs potential coincide with the Higgs potential parameters in the Higgs basis [16]

Minimization of the scalar potential, eq. (2.5), leads to the conditions [16]

$$
\begin{aligned}
\mu_1^2 &= -\frac{1}{2}\lambda_1 v^2 \\
\mu_3^2 &= \frac{1}{2}\lambda_6 v^2 .
\end{aligned}
\tag{2.6}
$$

These conditions can be used to eliminate μ_1^2 and μ_3^2 as independent variables from V.

Of the original ten scalar degrees of freedom, three Goldstone bosons ($G^\pm$ and G^0) are absorbed by the $W^\pm$ and Z^0. The remaining seven physical Higgs particles are: two CP-even (h^0 and H^0 with $m_{h^0} \leq m_{H^0}$), one CP-odd (A^0) and two charged Higgs pairs ($h_1^\pm$ and $h_2^\pm$).

In the basis $\mathbf{\Phi}^\dagger = (G^-, H^-, h^-)$ the squared-mass matrix for the charged Higgs states is given by

$$
\mathcal{M}_C^2 = \begin{pmatrix} 0 & 0 & 0 \\ 0 & M_{H^\pm}^2 & -\mu v/\sqrt{2} \\ 0 & -\mu v/\sqrt{2} & \mathcal{M}_{33}^2 \end{pmatrix} ,
\tag{2.7}
$$

where

$$
\begin{aligned}
M_{H^\pm}^2 &= \mu_2^2 + \frac{1}{2} v^2 \lambda_3 \\
\mathcal{M}_{33}^2 &= \mu_h^2 + \frac{1}{2} v^2 \lambda_8 .
\end{aligned}
\tag{2.8}
$$

The matrix element $M_{H^\pm}^2$ corresponds to the squared-mass of the charged scalars ($H^\pm$) that in the absence of the $SU(2)_L$ singlets $h^\pm$ would be physical Higgs particles.

The squared-mass matrix $\mathcal{M}_C^2$ can be diagonalized by the rotation matrix

$$
R = \begin{pmatrix} 1 & 0 & 0 \\ 0 & \cos\varphi & \sin\varphi \\ 0 & -\sin\varphi & \cos\varphi \end{pmatrix} .
\tag{2.9}
$$

where the angle φ characterize the size of the $H^\pm - h^\pm$ mixing.

JHEP08(2006)036

The mass eigenstate basis in the charged Higgs sector is defined as $\mathbf{H}^\dagger = (G^-, h_1^-, h_2^-)$ and the rotation angle is given by

$$\sin 2\varphi = \frac{\sqrt{2}v\mu}{M_2^2 - M_1^2}. \tag{2.10}$$

Here M_1 and M_2 stand for the masses of the scalars $h_1^\pm$ and $h_2^\pm$ which are given by

$$M_{1,2}^2 = \frac{1}{2}\left(M_{H^\pm}^2 + \mathcal{M}_{33}^2 \mp \sqrt{(M_{H^\pm}^2 - \mathcal{M}_{33}^2)^2 + 2\mu^2 v^2}\right). \tag{2.11}$$

In the Higgs basis the squared-masses for the CP-odd and CP-even Higgs states are given by [16]

$$\begin{aligned} M_{A^0}^2 &= M_{H^\pm}^2 - \frac{1}{2}v^2(\lambda_5 - \lambda_4) \\ M_{H^0,h^0}^2 &= \frac{1}{2}\left[M_{A^0}^2 + v^2(\lambda_1+\lambda_5) \pm \sqrt{[M_{A^0}^2 + v^2(\lambda_5 - \lambda_1)]^2 + 4v^4\lambda_6^2}\right] \end{aligned} \tag{2.12}$$

3. Charged scalar phenomenology

3.1 Cross section

In the following we discuss charged scalar $h_k^\pm$ $(k = 1, 2)$ production at a future e^+e^- collider. $h_k^\pm$ are produced in e^+e^- annihilation via s-channel exchange of a γ or Z^0 [2]. The total cross section for the process $e^+e^- \to h_k^+ h_k^-$ will be the sum of three terms

$$\sigma_{\text{total}} = \sigma_\gamma + \sigma_Z + \sigma_{\gamma Z} \tag{3.1}$$

corresponding to the pure photon, pure Z and photon–Z interference contributions respectively. Thus

$$\sigma_\gamma = \frac{1}{48\pi}\beta^3 (g\, s_w)^4 \frac{1}{s} \tag{3.2}$$

$$\sigma_Z = \frac{1}{3072\pi}\beta^3 \frac{g^4}{c_w^4}(W_{1k}^2 - 2s_w^2)^2[(-1+4s_w^2)^2+1] \frac{s}{(s-M_Z^2)^2 + M_Z^2\Gamma_Z^2} \tag{3.3}$$

$$\sigma_{Z\gamma} = -\frac{1}{192\pi}\beta^3 \frac{g^4 s_w^2}{c_w^2}(W_{1k}^2 - 2s_w^2)(-1+4s_w^2) \frac{s - M_Z^2}{(s-M_Z^2)^2 + M_Z^2\Gamma_Z^2}. \tag{3.4}$$

where $s_w = \sin\theta_w$, $c_w = \cos\theta_w$,

$$\beta = \sqrt{1 - 4\frac{M_k^2}{s}} \tag{3.5}$$

and $W_{11} = W_{22} = \cos\varphi$ and $W_{12} = -W_{21} = \sin\varphi$.

[2]There is also a t-channel Yukawa production through neutrino exchange but due to the smallness of this contribution to the total production cross section we do not consider it here.

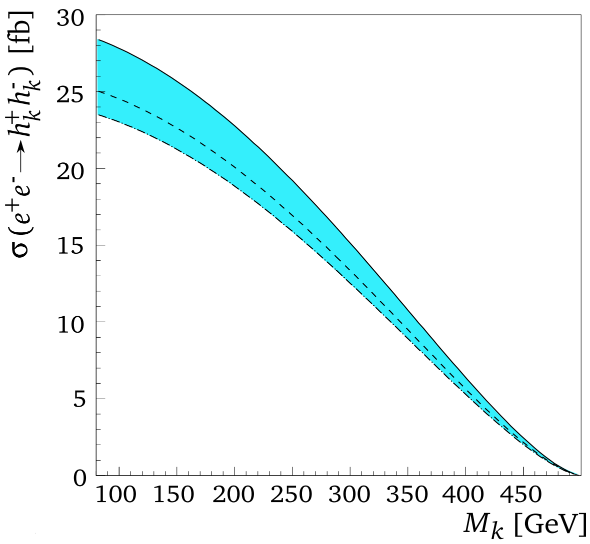

Figure 1: Production cross section for charged scalars $h_k^\pm$ at an 1 TeV e^+e^- collider with unpolarized beams.

From eqs. (2.8), (2.11) and (2.12) it can be noted that fixing $M_{1,2}$ does not fix M_{H^0,h^0} and M_{A^0}. Therefore, it is possible to take $M_{1,2}$ and W_{1k} as free parameters without being in conflict with LEP bounds for the CP-even and CP-odd Higgs masses [18 – 20].

In figure 1 we show the cross section at an 1 TeV e^+e^- collider with unpolarized beams. There we have taken 80 Gev $\leq M_k \leq$ 500 GeV. The spread in the plot is due to the dependence of the cross sections on φ. It is important to notice that for small (large) values of φ the cross section for h_1^+ increases (decreases) while the cross section for h_2^+ decreases (increases). Figure 1 illustrates the situation for the case $\varphi = 0$. In that case h_1^+ coincides with the SU(2) doublet H^+ (solid line) and h_2^+ with the SU(2) singlet h^+ (dashed line). The dotted-dashed line corresponds to $\cos\varphi \simeq 0.6$.

In figure 1 it can be seen that up to a mass of ~ 350 GeV the charged scalars have a cross section larger than 10 fb. Assuming an integrated luminosity of 1 ab^{-1} this implies that at least 10^4 charged scalar pairs will be produced.

3.2 Decay Widths

The Lagrangian in eq. (2.2) is written in the generic basis. From The SO(2) transformations in eq. (2.4) we have

$$\frac{v}{\sqrt{2}}\Pi_1' = \frac{v_1}{\sqrt{2}}\Pi_1 + \frac{v_2}{\sqrt{2}}\Pi_2. \tag{3.6}$$

Clearly Π_1' can be chosen real and diagonal and we can define the charged lepton mass eigenstates as

$$\widehat{M}_\ell = \frac{1}{\sqrt{2}}\sum_a v_a \Pi_a. \tag{3.7}$$

Similarly

$$\Pi_2' = -\Pi_1 \sin\beta + \Pi_2 \cos\beta. \tag{3.8}$$

Using eq. (3.7) we have

$$O \equiv \Pi_2' = -\sqrt{2}\frac{\tan\beta}{v}\widehat{M}_\ell + \frac{1}{\cos\beta}\Pi_2. \tag{3.9}$$

The couplings Π_1' and O are SO(2) invariants [16, 17]. In fact, the charged Higgs-fermion interaction Lagrangian (eq. (2.2)) written in terms of the fermions and Higgs physical masses can be written as

$$\begin{aligned} -\mathcal{L}_Y \supset\ & \bar{\nu}_{Li'} O_{i'j} e_{Rj} (\cos\varphi h_1^+ - \sin\varphi h_2^+) \\ & + (\nu_{Li})^T C (2 f_{ij}) e_{Lj} (\sin\varphi h_1^+ + \cos\varphi h_2^+) + \text{H.c.} \end{aligned} \tag{3.10}$$

Notice also that in the Higgs basis $\widehat{M}_\ell = (v/\sqrt{2})\Pi_1$ ($\Pi_1' = \Pi_1$) and $O = \Pi_2$.

By construction Π_1' is a real diagonal matrix, and the resulting charged lepton mass matrix is then diagonal. It does not appear in the fermion-charged Higgs interaction Lagrangian. Similarly $O \equiv \Pi_2'$ is non-diagonal in the charged lepton mass eigenstate basis and generate neutral Higgs-mediated FCNC at tree level. Thus, for a phenomenologically acceptable theory the off-diagonal elements of O must be small. Typically, these couplings are in conflict with experimental bounds on FCNC processes. However, even in the case of the most general Higss-fermion couplings there are parameter regions where FCNC effects are under control. Usually this corresponds to a matrix O that follows the same hierarchy of the charged lepton mass matrix [21]. In our case this corresponds to the situation where O_{33} is large. However, with some fine-tuning in eq. (3.9), it is also possible to have regions with O_{33} smaller than the others O_{ij} and compatible with FCNC experimental constraints. In the absence of neutrino physics this regions should seem unjustified.

The fine-tuning required in eq. (3.9), when O_{33} is small, can be parameterized through new $\tan\beta$-like parameters which are basis independent [16, 17]. In the case of the charged Higgs-fermion interactions $\tan\beta$ never appears. However, one can define various $\tan\beta$-like parameters that can be identified with ratios of physical couplings. For the leptonic sector we have [16, 17]

$$\tan\beta_E = -\frac{O_{33}}{(\Pi_1')_{33}}, \tag{3.11}$$

which measures the hierarchy deviation of O with respect to the charged lepton mass matrix. In terms of the generic basis parameters we have

$$\begin{aligned} \tan\beta_E &= -\frac{1}{\sqrt{2}}\frac{v}{m_\tau}O_{33} & (3.12) \\ &= \tan\beta - \frac{1}{\sqrt{2}\cos\beta}\frac{v}{m_\tau}\Pi_2 & (3.13) \end{aligned}$$

Note that even for usual values of $\tan\beta$, we can have $|\tan\beta_E| \ll 1$. In the same way it is possible to define $\tan\beta_D$, $\tan\beta_U$. In some special cases as in the 2HDM of type-II, these parameters are reduced to the usual $\tan\beta$. Moreover, in the most general case, these, $\tan\beta$-like, parameters are not necessarily equal, i.e., $\tan\beta_E \neq \tan\beta_D \neq \tan\beta_U$.

Charged scalars $h_{1,2}^+$ will decay through the couplings O_{ij} and f_{ij}. Possible leptonic final states are $\nu_i \ell_j^+$. Possible final states involving quarks are $\bar{d}_i u_j$. These decays are

JHEP08(2006)036

Process	Constraint
$\mu^- \to e^+e^-e^-$	$\|O_{12}O_{11}\| < 3.6\times10^{-7}\left(\frac{M_h^0}{100\mathrm{GeV}}\right)^2$
$\tau^- \to e^+e^-e^-$	$\|O_{13}O_{11}\| < 1.3\times10^{-3}\left(\frac{M_h^0}{100\mathrm{GeV}}\right)^2$
$\tau^- \to \mu^+\mu^-\mu^-$	$\|O_{13}O_{12}\| < 0.9\times10^{-3}\left(\frac{M_h^0}{100\mathrm{GeV}}\right)^2$
$\tau^- \to \mu^-\mu^-e^+$	$\|O_{23}O_{21}\| < 0.9\times10^{-3}\left(\frac{M_h^0}{100\mathrm{GeV}}\right)^2$
$\tau^- \to e^-\mu^-e^+$	$\|O_{13}O_{21}+O_{23}O_{11}\| < 1.0\times10^{-3}\left(\frac{M_h^0}{100\mathrm{GeV}}\right)^2$
$\tau^- \to e^-\mu^-\mu^+$	$\|O_{13}O_{22}+O_{23}O_{12}\| < 1.0\times10^{-3}\left(\frac{M_h^0}{100\mathrm{GeV}}\right)^2$
$\mu^- \to e^-\gamma$	$\|O_{12}O_{11}+O_{22}O_{21}+O_{32}O_{31}\| < 4.1\times10^{-5}\left(\frac{M_h^0}{100\mathrm{GeV}}\right)^2$
$\tau^- \to e^-\gamma$	$\|O_{13}O_{11}+O_{23}O_{21}+O_{33}O_{31}\| < 4.7\times10^{-2}\left(\frac{M_h^0}{100\mathrm{GeV}}\right)^2$
$\tau^- \to \mu^-\gamma$	$\|O_{13}O_{12}+O_{23}O_{22}+O_{33}O_{32}\| < 3.3\times10^{-2}\left(\frac{M_h^0}{100\mathrm{GeV}}\right)^2$

Table 1: Constraints on the parameters O_{ij} from tree level and radiative FCNC processes induced by the neutral Higgs h^0.

determined by the couplings O^q_{ij} where, in general

$$O^q = -\sqrt{2}\frac{\tan\beta}{v}\widehat{M}_q + \frac{1}{\cos\beta}\Pi^q_2. \tag{3.14}$$

Here q refers to up-type and down-type quarks, $\widehat{M}_q$ are the diagonal quark mass matrices, and Π^q_2 are 3×3 Yukawa coupling matrices of the second Higgs doublet. Notice that in the Higgs basis $\widehat{M}_\ell = (v/\sqrt{2})\Pi_1$ and $O = \Pi_2$.

We are interested in the widths and branching ratios for leptonic final states. The Lagrangian (3.10) determines the two body decays $h^+_{1,2} \to (\sum_i \nu_i)\ell^+_j$. The decay rate reads

$$\Gamma(h^+_k \to (\sum_i \nu_i)\ell^+_j) = \frac{M_k}{16\pi}\sum_i [O^2_{ij}W^2_{1k} + (2f_{ij})^2 W^2_{2k}]\,. \tag{3.15}$$

The couplings $h^+_k W^- Z$ and $h^+_k W^-\gamma$ do not exist in the Zee model. This can be understood as follows: since h^+_k is a mixture of H^+ and h^+ these couplings are determined by the SU(2) doublet component. However, in the 2HDM of type-III these vertices do not exist [22]. Therefore the decays $h^+_k \to W^+\gamma$, W^+Z^0 in the Zee model are not present at tree level. For this reason we do not consider them.

4. Constraints from FCNC processes

In the GZM FCNC interactions are induced by the charged and neutral Higgses. Bounds on the $O_{ji}O_{km}$ couplings can be obtained from the non-observation of tree-level processes $\ell^-_i \to \ell^+_j\ell^-_k\ell^-_m$. Constraints on $O_{ki}O_{kj}$ come from radiative processes $\ell^-_i \to \ell^-_j\gamma$ induced by neutral Higgses. Limits on $f_{ik}f_{kj}$ and on $O_{ki}f_{kj}$ couplings come from radiative processes mediated

Process	Constraint
$\mu^- \to e^-\gamma$	$\lvert f_{23}f_{13}\rvert < 4.1\times10^{-5}\left(\frac{M_1}{100\mathrm{GeV}}\right)^2$
$\tau^- \to e^-\gamma$	$\lvert f_{23}f_{12}\rvert < 4.7\times10^{-2}\left(\frac{M_1}{100\mathrm{GeV}}\right)^2$
$\tau^- \to \mu^-\gamma$	$\lvert f_{13}f_{12}\rvert < 3.3\times10^{-2}\left(\frac{M_1}{100\mathrm{GeV}}\right)^2$

Table 2: Constraints on the parameters f_{ij} coming from radiative FCNC processes induced by the charged Higgs $h_1^\pm$.

by charged scalars[3]. An important remark is that once the constraints on the $f_{ik}f_{kj}$ and $O_{ki}O_{kj}$ couplings are satisfied the limits on $O_{ki}f_{kj}$ are no longer important, for this reason we do not list them. Table 1 shows the constraints coming from the processes mediated by neutral scalars. Table 2 summarize the limits on the f_{ij} parameters. Experimental constraints used in both tables were taken from [23]

5. Neutrino physics

5.1 Neutrino mass matrix in the GZM

In this section we will discuss the neutrino mass matrix. The Majorana neutrino mass matrix in the Zee model arises at the one loop level through the exchange of the scalars $h_1^\pm$ and $h_2^\pm$ as shown in figure 2. Assuming $M_1, M_2 \gg m_e, m_\mu, m_\tau$ we have

$$(M_\nu)_{ii'} = \kappa[f_{ij}(\widehat{M_\ell})_{jj}O_{i'j} + O_{ij}(\widehat{M_\ell})_{jj}f_{i'j}] \tag{5.1}$$

where

$$\kappa = \frac{\sin 2\varphi}{(4\pi)^2}\ln\left(\frac{M_2^2}{M_1^2}\right). \tag{5.2}$$

5.2 Neutrino Mass Matrix in the NMZM

In this section we discuss the neutrino mass matrix in the context of the NMZM. In our scheme the neutrino mass matrix is assumed to be

$$M_\nu = \kappa\begin{pmatrix} M_{ee} & M_{e\mu} & M_{e\tau} \\ M_{e\mu} & 0 & M_{\mu\tau} \\ M_{e\tau} & M_{\mu\tau} & 0 \end{pmatrix}. \tag{5.3}$$

The neutrino mass matrix, can be diagonalized by a matrix U, which can be parametrized as

$$U = \begin{pmatrix} 1 & 0 & 0 \\ 0 & c_{23} & s_{23} \\ 0 & -s_{23} & c_{23} \end{pmatrix} \times \begin{pmatrix} c_{13} & 0 & s_{13} \\ 0 & 1 & 0 \\ -s_{13} & 0 & c_{13} \end{pmatrix} \times \begin{pmatrix} c_{12} & s_{12} & 0 \\ -s_{12} & c_{12} & 0 \\ 0 & 0 & 1 \end{pmatrix}, \tag{5.4}$$

where $s_{ij} = \sin\theta_{ij}$ and $c_{ij} = \cos\theta_{ij}$. Phases are zero since only real parameters are considered.

[3]These processes also give bounds on $O_{ik}O_{kj}$. However they are weaker than those coming from radiative processes mediated by neutral Higgses.

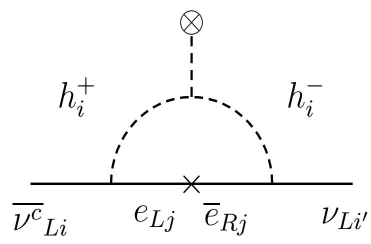

Figure 2: Loop diagrams for Majorana neutrino mass. Here $i = 1, 2$

From

$$U^T M_\nu U = \widehat{M_\nu}, \tag{5.5}$$

and taking the limit $\sin^2\theta_{13} = 0$, since experimental neutrino data require $\sin^2\theta_{13}$ to be small [14], we can find approximate analytical expressions for the atmospheric and solar mixing angle as well as for Δm^2_{23}:

$$\begin{aligned} \tan^2\theta_{23} &\simeq \left(\frac{M_{e\tau}}{M_{e\mu}}\right)^2, \\ \tan 2\theta_{12} &\simeq \sqrt{2}\frac{M_{e\mu} - M_{e\tau}}{M_{ee} + M_{\mu\tau}}, \\ \sqrt{\Delta m^2_{23}} &\simeq \frac{\kappa}{\sqrt{2}}(M_{e\mu} - M_{e\tau}). \end{aligned} \tag{5.6}$$

Due to our two-zero-texture mass matrix (eq. (5.3)) we have an inverted hierarchy neutrino mass spectrum [24] and therefore $M_{ee} \simeq M_{\mu\tau}$. Thus the neutrino mass matrix, eq. (5.3), has only three independent entries which, from eqs. (5.6), can be written in terms of $\tan^2\theta_{23}$, $\tan 2\theta_{12}$ and Δm^2_{23}, namely

$$\begin{aligned} M_{ee} &\simeq M_{\mu\tau} \simeq \frac{\sqrt{\Delta m^2_{23}}}{\kappa \tan 2\theta_{12}}, \\ M_{e\mu} &\simeq \frac{\sqrt{2\Delta m^2_{23}}}{\kappa(1 + \tan\theta_{23})}, \\ M_{e\tau} &\simeq -\frac{\tan\theta_{23}\sqrt{2\Delta m^2_{23}}}{\kappa(1 + \tan\theta_{23})}. \end{aligned} \tag{5.7}$$

FCNC experimental constraints are usually satisfied by assuming that O follows the same hierarchy of the charged leptons mass matrix. Under this assumption the O_{i1} elements can be neglected. For the more general structure of O, in order to neglect the O_{i1} parameters, it is sufficient to assume that that they are not too much larger than the others O_{ij}. Therefore in any case terms proportional to m_e, in the neutrino mass matrix, (see eq. (5.1)) can be neglected. Thus we obtain eq. (5.3) with $O_{23} = O_{32} = 0$. Under this constraint the mass matrix depends on κ and on the seven parameters

$$f_{12}, f_{13}, f_{23}, O_{12}, O_{13}, O_{22}, O_{33}, \tag{5.8}$$

as can be seen from eqs. (5.1) and (5.3). By using equations in (5.7) we can write four of these parameters in terms of the other three. Equations (A.1), (A.2), (A.3) and (A.4), in the appendix, give the expressions for f_{12}, f_{13}, f_{23}, O_{13}, in terms of O_{12}, O_{22}, and O_{33}. Note that both f_{23} and O_{33} must be different from zero.

Next we will consider the cases for which eqs. (A.1), (A.2), (A.3) and (A.4) can be expressed in terms of a single parameter. We will call these cases the one-parameter solutions. Since O_{33} cannot be zero (see eq. (A.2)) we will parametrize all our one-parameter solutions in terms of this coupling. This leaves us with only four possibilities: $O_{12} = 0$, $O_{13} = 0$, $f_{12} = 0$, $f_{13} = 0$ and the remaining parameters in eq. (5.8) different from zero in each case. We will show below that the first two lead to solutions with large O_{33}, while the last two lead to solutions with small O_{33}.

5.3 The one-parameter region

The main point here is that in these two cases (small and large O_{33}) not only neutrino physics but the decay patterns of $h_1^{\pm}$ are governed by a single parameter. This allows an analytical approach to the problem of identifying a particular collider signature that allows to distinguish between different regions in parameter space. In the following we will discuss the four possibilities mentioned previously and we will estimate the values of the parameters, consistent with neutrino physics as well as with FCNC constraints, in each case. This discussion will be useful in our analysis of the decays of h_1^+ presented in section 6.2.

5.3.1 The large O_{33} case

Choosing $O_{12} = 0$ and $O_{22} = (m_\mu/m_\tau)O_{33}$, as in references [12, 13], eqs. (A.1), (A.2), (A.3) and (A.4) are reduced to the one-parameter solution

$$\begin{aligned}
f_{12} \approx& \frac{\left[1 + \left(2 + 4\,\tan^2 2\theta_{12}\right)\,\tan\theta_{23} + \tan^2\theta_{23}\right]}{2\sqrt{2}\,\kappa\,\tan^2 2\theta_{12}\,\tan\theta_{23}\,(1+\tan\theta_{23})} \frac{\sqrt{\Delta m^2_{23}}\,m_\tau}{m_\mu^2}\frac{1}{O_{33}} \sim \frac{6.3\times 10^{-9}}{\kappa\, O_{33}}, \\
f_{13} \approx& -\frac{\sqrt{2}\,\tan\theta_{23}}{\kappa\,(1+\tan\theta_{23})}\frac{\sqrt{\Delta m^2_{23}}}{m_\tau}\frac{1}{O_{33}} \sim -\frac{1.9\times 10^{-11}}{\kappa\, O_{33}}, \\
f_{23} \approx& \frac{1}{\kappa\,\tan 2\theta_{12}}\frac{\sqrt{\Delta m^2_{23}}}{m_\tau}\frac{1}{O_{33}} \sim \frac{1.2\times 10^{-11}}{\kappa\, O_{33}}, \\
O_{13} \approx& -\frac{1+\tan\theta_{23}}{2\sqrt{2}\,\tan 2\theta_{12}\,\tan\theta_{23}} O_{33} \sim -0.3\, O_{33}.
\end{aligned} \tag{5.9}$$

The last values in each equation are obtained using the best fit point value for each neutrino observable.

An upper bound for κ can be estimated using the fact that

$$\kappa = \frac{\sin 2\varphi}{(4\pi)^2}\ln\left(\frac{M_2^2}{M_1^2}\right) = \frac{\sqrt{2}v\mu}{(4\pi)^2}\frac{1}{M_2^2 - M_1^2}\ln\left(\frac{M_2^2}{M_1^2}\right) \simeq \frac{\sqrt{2}}{(4\pi)^2}\frac{v\mu}{M_2^2}. \tag{5.10}$$

Therefore for $M_2 < 1000\,\text{GeV}$ and $|\mu| < 500\,\text{GeV}$ [25], we have that $|\kappa| \lesssim 10^{-2}$. For example for $M_1 = 200\,\text{GeV}$, $M_2 = 300\,\text{GeV}$, and $\mu = 100\,\text{GeV}$, we have

$$\sin 2\varphi = 0.7 \qquad \text{and} \qquad \kappa = 3.6\times 10^{-3}. \tag{5.11}$$

On the other hand, from the expression for f_{12} in eq. (5.9) and imposing $f_{12} \lesssim 10^{-2}$ a lower bound on κ can be found. Choosing $O_{33} \lesssim 10^{-2}$, we have that $|\kappa| \gtrsim 10^{-5}$. For example, for $\mu = 2\,\mathrm{GeV}$ and with M_1 and M_2 as in the previous case, we have

$$\sin 2\varphi = 0.014 \qquad \text{and} \qquad \kappa = 7.2 \times 10^{-5}. \tag{5.12}$$

Using the value of κ given in eq. (5.11) we have

$$f_{12} \sim \frac{1.8 \times 10^{-6}}{O_{33}}, \qquad f_{13} \sim -\frac{5.2 \times 10^{-9}}{O_{33}}, \qquad f_{23} \sim \frac{3.2 \times 10^{-9}}{O_{33}}. \tag{5.13}$$

Now instead of $O_{12} = 0$ we choose $O_{13} = 0$. Again, as in the previous case, we take $O_{22} = (m_\mu/m_\tau)O_{33}$ and the best fit point values for each neutrino observable. With κ given by (5.11), eqs. (A.1), (A.2), (A.3) and (A.4) become

$$f_{12} \sim \frac{1.5 \times 10^{-6}}{O_{33}},\ f_{13} \sim -\frac{5.2 \times 10^{-9}}{O_{33}},\ f_{23} \sim \frac{3.2 \times 10^{-9}}{O_{33}},\ O_{12} \sim 0.02\, O_{33}, \tag{5.14}$$

which is basically the same result obtained in the case with $O_{12} = 0$ (eqs. (5.13)).

From eqs. (5.13) and (5.14) it can be seen that all the parameters can be below 10^{-3}, with a hierarchy of order 10^3 between f_{12} and the others f_{ij}. In this way the constraints on the couplings coming from FCNC interactions (tables 1 and 2) are always satisfied.

Note that $f_{12} \lesssim 10^{-2}$ requires $O_{33} \gtrsim 10^{-4}$. Therefore the range of variation of O_{33} is restricted to $10^{-4} \lesssim O_{33} \lesssim 10^{-2}$. For κ small, as in eq. (5.12), $O_{33} \sim 10^{-2}$. Note that in this region the values of $\tan\beta_E$ are compatible with the usual $\tan\beta$ values of the 2HDM of type-II. In particular this region is compatible with the three $\tan\beta$-like parameters being equal.

5.3.2 The small O_{33} case

If we choose $f_{13} = 0$ and, in order to define the one-parameter solution in this case[4] $O_{22} = 0$, eqs. (A.1), (A.2), (A.3) and (A.4) become

$$\begin{aligned}
f_{12} &\approx \frac{(1+\tan\theta_{23})}{2\sqrt{2}\,\kappa\,\tan 2\theta_{12}^2\,\tan\theta_{23}}\frac{\sqrt{\Delta m_{23}^2}}{m_\tau}\frac{1}{O_{33}} \sim \frac{3.6 \times 10^{-12}}{\kappa\, O_{33}},\\
f_{23} &\approx \frac{1}{\kappa\,\tan 2\theta_{12}}\frac{\sqrt{\Delta m_{23}^2}}{m_\tau}\frac{1}{O_{33}} \sim \frac{1.2 \times 10^{-11}}{\kappa\, O_{33}},\\
O_{12} &\approx \frac{\sqrt{2}\,\tan 2\theta_{12}\,\tan\theta_{23}}{(1+\tan\theta_{23})}\frac{m_\tau}{m_\mu}O_{33} \sim 27\, O_{33},\\
O_{13} &\approx \frac{\sqrt{2}\,\tan 2\theta_{12}}{1+\tan\theta_{23}}O_{33} \sim 1.6\, O_{33}.
\end{aligned} \tag{5.15}$$

The last values in each equation are obtained using the best fit point values for each neutrino observable. Note that $O_{12} \lesssim 10^{-2}$ requires $O_{33} \lesssim 4 \times 10^{-4}$.

[4]This choice allow us to define the one-parameter solutions. However, we stress that our results does not depend on this choice. Our main conclusions hold for any $O_{22} < O_{33}$.

Case	O_{33}	κ	μ (GeV)
Large O_{33}	$10^{-4} - 10^{-2}$	$10^{-5} - 10^{-2}$	$2 - 500$
Small O_{33}	$10^{-7} - 4 \times 10^{-3}$	$3 \times 10^{-6} - 10^{-2}$	$0.2 - 500$

Table 3: Range of O_{33}, κ and μ for the one-parameter solutions in the NMZM

On the other hand, from the expression for f_{23} in eq. (5.15), if $O_{33} \lesssim 4 \times 10^{-4}$ and we impose the bound $f_{23} \lesssim 10^{-2}$ we have that $\kappa \gtrsim 3 \times 10^{-6}$. For example, if we choose $\mu = 0.2\,\text{GeV}$, $M_1 = 200\,\text{GeV}$ and $M_2 = 300\,\text{GeV}$, we have

$$\sin 2\varphi = 1.4 \times 10^{-3} \qquad \text{and} \qquad \kappa = 7.2 \times 10^{-6} \tag{5.16}$$

For the value of κ given in eq. (5.11), that satisfies the bound $\kappa \gtrsim 3 \times 10^{-6}$, with $M_1 = 200$ GeV and $M_2 = 300\,\text{GeV}$ we have

$$f_{12} \sim \frac{1 \times 10^{-9}}{O_{33}}, \quad f_{23} \sim \frac{3.2 \times 10^{-9}}{O_{33}}. \tag{5.17}$$

Now instead of $f_{13} = 0$ we choose $f_{12} = 0$. Using the best fit point values for each neutrino observable, $O_{22} = 0$ and κ given by eq. (5.11), eqs. (A.1), (A.2), (A.3) and (A.4) become

$$f_{13} \sim \frac{9.8 \times 10^{-10}}{O_{33}},\ f_{23} \sim \frac{3.2 \times 10^{-9}}{O_{33}},\ O_{12} \sim 32\,O_{33},\ O_{13} \sim 1.6\,O_{33}. \tag{5.18}$$

In both cases ($f_{12} = 0$ or $f_{13} = 0$) we can have all the five parameters of order of 10^{-4} without any hierarchy among them. In fact, the case $f_{12} = 0$, considered here, is a particular case of the one studied in reference [11] in which all the parameters O_{ij} and f_{ij} are of the same order of magnitude. From tables 1 and 2 it can be seen that FCNC constraints are always satisfied.

A lower bound on O_{33} can be obtained using the bound $f_{23} \lesssim 10^{-2}$. Together with the upper bound estimated previously we have $10^{-7} \lesssim O_{33} \lesssim 4 \times 10^{-3}$. Notice that for smaller values of κ, as the one in eq. (5.16), the range of variation is more restricted, $10^{-5} \lesssim O_{33} \lesssim 4 \times 10^{-3}$. Note that in this region $|\tan\beta_E|$ is small. Therefore, in this region large differences among the three $\tan\beta$-like parameters are expected. These three parameters are indeed SO(2)-invariant quantities, and thus corresponds to physical observables that can be measured [17]. If these parameters are found to be close in value, the small O_{33} region should be excluded.

It is worth noticing that there are no more possibilities in the one-parameter solution case. The large O_{33} case, obtained when either O_{12} or O_{13} are neglected implies a hierarchy among the non zero f_{ij} and, depending on the case, on O_{12} or O_{13}. In the small O_{33} case, obtained when either f_{12} or f_{13} are neglected, it is possible to have all the parameters at the level of 10^{-4}. Table 3 shows the allowed range of variation for O_{33}, κ and μ in each case.

6. Neutrino and collider physics

6.1 Determination of the neutrino mass matrix parameters

In this section we discuss how the charged scalar decays can give some hints about the parameters that determine neutrino masses and mixing angles. Charged Higgs decays are governed by the same parameters that control neutrino physics so, in principle, the information coming from these decays can be used to reconstruct the neutrino mass matrix. Outside of the one-parameter regions analysed in section 5 the number of parameters is large and since neutrino flavour cannot be determined the mass matrix cannot be, in general, reconstructed. Despite this, in the limiting case of small mixing ($\varphi \ll 1$), the fact that the the mainly doublet state decays are dictated by the O_{ij} and the mainly singlet state decays are controlled by the f_{ij} leads to a situation in which the reconstruction of part of the parameter space of the model is possible.

The charged scalar singlet h^+ does not couples to quarks. Thus experimentally the mainly singlet state can be differentiated from the mainly doublet state by the fact that the branching ratio to final states with quarks ($\bar{u}_i d_j$) must be smaller for the former than for the latter. Our main assumption here is that all the decays that we are going to consider have a branching ratio in the order of at least per-mille.

In the following discussion we will use the notation $h^+_{d,s}$ for charged Higgses. Here d and s denote the mainly doublet and mainly singlet states respectively. Note that $d = 1$, $s = 2$ or $d = 2$, $s = 1$ are possible. Ratios of branching ratios for $h^+_{d,s}$ can be used to obtain information about the O_{ij} and f_{ij} couplings. In the case of h^+_d we have

$$\frac{Br(h^+_d \to (\sum_i \nu_i)\ell^+_j)}{Br(h^+_d \to (\sum_k \nu_k)\ell^+_s)} \simeq \frac{\sum_i O^2_{ij}}{\sum_k O^2_{ks}} \tag{6.1}$$

and for h^+_s

$$\frac{Br(h^+_s \to (\sum_i \nu_i)\ell^+_j)}{Br(h^+_s \to (\sum_k \nu_k)\ell^+_s)} \simeq \frac{\sum_i f^2_{ij}}{\sum_k f^2_{ks}}. \tag{6.2}$$

Corrections to both ratios are $\propto \varphi^2 \lll 1$. The interesting point here is that despite the large number of parameters the relative size of the f_{ij} couplings can be obtained by suitable combinations of ratios of branching ratios, for example

$$\frac{Br^\mu_s - Br^\tau_s + Br^e_s}{Br^\mu_s - Br^e_s + Br^\tau_s} \simeq \frac{f^2_{12}}{f^2_{23}} \tag{6.3}$$

with $Br^{\ell_j}_s$ denoting $Br(h^+_s \to (\sum_i \nu_i)\ell^+_j)$. For the O_{ij} the situation is more complicated but even in this case some information can be obtained from the ratios of branching ratios. For example, the relation

$$\frac{Br(h^+_d \to (\sum_i \nu_i)\mu^+)}{Br(h^+_d \to (\sum_k \nu_k)e^+)} \simeq \frac{O^2_{12} + O^2_{22}}{O^2_{11} + O^2_{21} + O^2_{31}} \tag{6.4}$$

allows to determine the relative importance of the couplings involved in these decays.

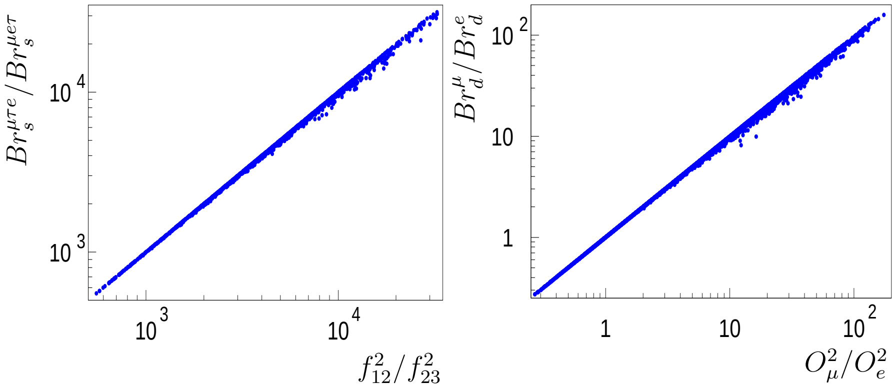

Figure 3: Ratio of branching ratios $Br_s^{\mu\tau e}/Br_s^{\mu e\tau} = (Br_s^\mu - Br_s^\tau + Br_s^e)/(Br_s^\mu - Br_s^e + Br_s^\tau)$ versus f_{12}^2/f_{23}^2 (left) and $Br_d^\mu/Br_d^e = Br(h_d^+ \to (\sum_i \nu_i)\mu^+)/Br(h_d^+ \to (\sum_k \nu_k)e^+)$ versus $O_\mu^2/O_e^2 = (O_{12}^2 + O_{22}^2)/(O_{11}^2 + O_{21}^2 + O_{31}^2)$ (right). See text.

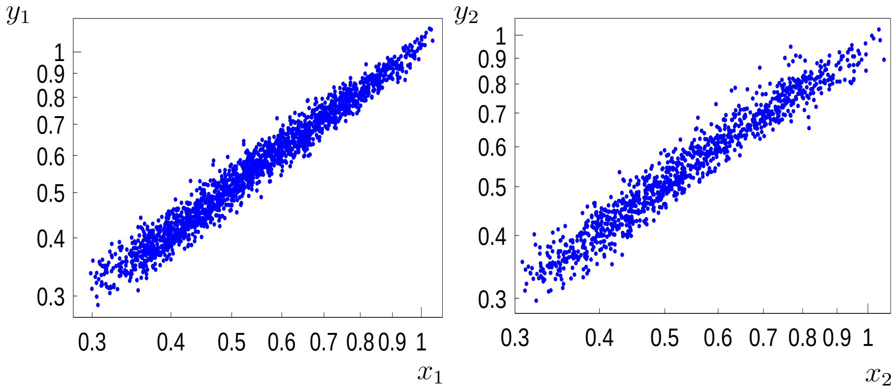

Figure 4: Ratio of branching ratios indicated by the variables y_1 (left) and y_2 (right) versus the atmospheric and solar mixing angles indicated by the variables x_1 (left) and x_2 (right). See text

Figure 3 shows the ratios of branching ratios described above. Any deviation from the small mixing assumption would lead to a large dispersion.

There are two limit cases of particular interest where the decays of $h_{d,s}^+$ are correlated with the neutrino mixing angles, $O_{12} \ll O_{13} \ll O_{22} < O_{33}$ or $O_{13} \ll O_{12} \ll O_{22} < O_{33}$. Figure 4 shows both cases. In the left plot the variables y_1 and x_1 are given by

$$y_1 = \sqrt{\frac{Br_s^\mu - Br_s^e + Br_s^\tau}{Br_s^e - Br_s^\mu + Br_s^\tau}} \left(1 - \frac{m_\mu}{m_\tau}\sqrt{\frac{Br(h_d^+ \to (\sum_i \nu_i)\mu^+)}{Br(h_d^+ \to (\sum_k \nu_k)\tau^+)}}\right)$$
$$x_1 = \frac{1}{\sqrt{2}\tan 2\theta_{12}}\left(1 + \frac{1}{\tan\theta_{23}}\right). \tag{6.5}$$

In the right one the variables y_2 and x_2 are defined as

$$y_2 = \sqrt{\frac{Br_s^\mu - Br_s^e + Br_s^\tau}{Br_s^\mu - Br_s^\tau + Br_s^e}} \left(\frac{m_\tau}{m_\mu}\sqrt{\frac{Br(h_d^+ \to (\sum_i \nu_i)\tau^+)}{Br(h_d^+ \to (\sum_k \nu_k)\mu^+)}} - 1\right)$$
$$x_2 = \frac{1}{\sqrt{2}\tan 2\theta_{12}}(1 + \tan\theta_{23}) \tag{6.6}$$

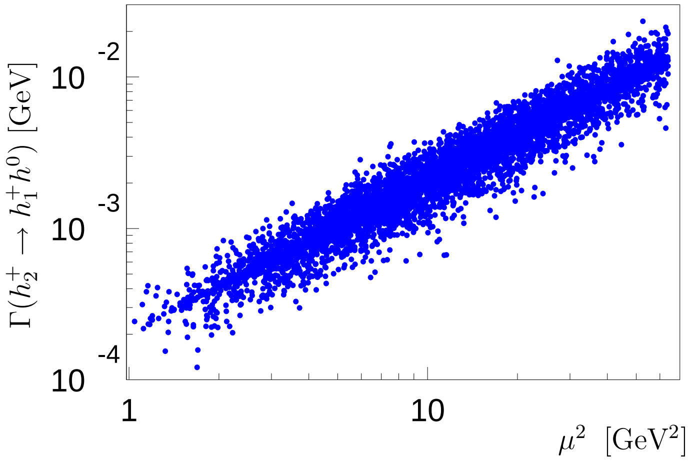

Figure 5: Decay rate $\Gamma(h_2^+ \to h_1^+ h^0)$ versus μ^2 for fixed values $M_2 = 400\,\text{Gev}$, $M_1 = 150\,\text{Gev}$ and $M_{h^0} = 130\,\text{GeV}$.

Another important decay, if kinematically allowed, that could be used to obtain information about μ is $h_2^+ \to h_1^+ h^0$. The decay rate for this process reads

$$\Gamma(h_2^+ \to h_1^+ h^0) = \frac{1}{16\pi} \frac{\Lambda^2}{M_2} \sqrt{1 - 4\frac{M_1^2}{M_2^2}}. \tag{6.7}$$

Here

$$\Lambda = \frac{\mu}{\sqrt{2}} \sin\alpha \cos 2\varphi + v\frac{\sin 2\varphi}{2}(\Lambda_{22} - \Lambda_{33}) \tag{6.8}$$

and

$$\begin{aligned} \Lambda_{22} &= \lambda_7 \cos\alpha - \lambda_3 \sin\alpha, \\ \Lambda_{33} &= \lambda_{10} \cos\alpha - \lambda_8 \sin\alpha \end{aligned} \tag{6.9}$$

where α is the mixing angle that define the two CP-even Higgs mass eigenstates, h^0 and H^0.

Figure 5 shows the decay rate $\Gamma(h_2^+ \to h_1^+ h^0)$ versus μ^2. There we have fixed $M_2 = 400\,\text{Gev}$, $M_1 = 150\,\text{Gev}$, $M_{h^0} = 130\,\text{GeV}$ and $\alpha = \pi/6$. μ is in the range $0.1\,\text{GeV} - 8\,\text{Gev}$ in order to ensure $\varphi \ll 1$. The dispersion is due to the presence of the other couplings, present in the scalar potential (eq. (2.5)). Apart from allowing the approximate determination of μ, measurements of $\Gamma(h_2^+ \to h_1^+ h^0)$ in the range indicated by figure 5 will indicate that the small mixing limit is realized.

As has been shown, in order to reconstruct the parameter space of the model, production of charged scalars and detection of di-lepton final states are necessary. At e^+e^- collider the main background for the signal $h_{s,d}^\pm \to \ell_j^\pm \nu$, comes from the W-boson decays $W^\pm \to \ell_j^\pm \nu$. However, as pointed out in reference [26], thanks to the different structure of the $h_{s,d}^\pm$ and $W^\pm$ electroweak interactions with charged leptons, the $\ell_j^\pm$ polarization is very different and will allow a separation of $h_{s,d}^\pm \to \ell_j \nu$ and $W^\pm \to \ell_j \nu$ on an statistical basis. In this way the branching ratios $Br(h_{s,d}^\pm \to (\sum_i \nu_i)\ell_j^\pm)$ should, in principle, be measured.

JHEP08(2006)036

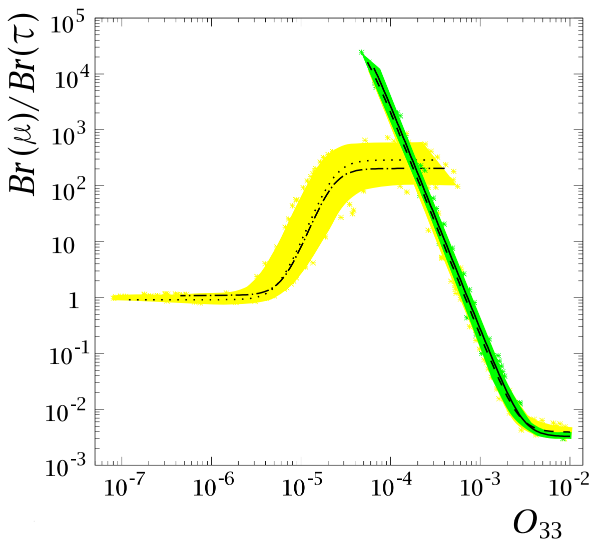

Figure 6: $Br(h_1^+ \to (\sum_i \nu_i)\mu^+)/Br(h_1^+ \to (\sum_i \nu_i)\tau^+)$ as a function of O_{33} for $3\times 10^{-6} < \kappa < 10^{-2}$ obtained with $0.2 < \mu < 500\,\mathrm{GeV}$, $M_1 = 200\,\mathrm{GeV}$ and $M_2 = 500\,\mathrm{GeV}$. All the parameters f_{ij} and O_{ij} satisfy the bounds shown in tables 1 and 2. For all the dark gray (green) points $O_{12} < 10^{-6}$. See text.

6.2 Hierarchy of charged Higgs leptonic decays

In this section we will show that in the NMZM, the decay process $h_1^+ \to (\sum_i \nu_i)\mu^+$ is enhanced in comparision to the 2HDM of type-I and type-II. Moreover, it is shown that in large parts of the parameter space, $h_1^+ \to (\sum_i \nu_i)\mu^+$ can be the dominant leptonic decay.

In the one-parameter solutions, described in section 5, the parameters O_{12}, O_{13}, f_{12}, f_{13} and f_{23} are governed by the parameter O_{33}. In this way the $Br(h_1^+ \to (\sum_i \nu_i)\ell_j^+)$ are functions of O_{33}. In order to find expressions with no dependence on κ or O_{33} and correlated with neutrino physics observables ($\tan 2\theta_{12}$, $\tan\theta_{23}$) we consider ratios of branching ratios in the limits $O_{ij} \gg f_{ij}$ and $O_{ij} \ll f_{ij}$, namely

$$\frac{Br(h_1^+ \to (\sum_i \nu_i)\mu^+)}{Br(h_1^+ \to (\sum_i \nu_i)\tau^+)} = \frac{\sum_i[(O_{i2}\cos\varphi)^2 + (2f_{i2}\sin\varphi)^2]}{\sum_i[(O_{i3}\cos\varphi)^2 + (2f_{i3}\sin\varphi)^2]} \tag{6.10}$$

$$\approx \begin{cases} \dfrac{\sum_i O_{i2}^2}{\sum_i O_{i3}^2} & \text{for } O_{ij} \gg f_{ij} \\[2ex] \dfrac{\sum_i f_{i2}^2}{\sum_i f_{i3}^2} & \text{for } O_{ij} \ll f_{ij} \end{cases} \tag{6.11}$$

Clearly from eqs. (5.9) or (5.15), eq. (6.11) depend only on the neutrino mixing angles and charged lepton masses. We will call the regions of parameter space with either O_{ij} or f_{ij} dominance correlation regions. Ratio of branching ratios in these regions are κ independent (or μ independent). In general, outside the correlation regions, the independence on μ approximately holds, but there is a dependence on M_2.

Figure 6 shows the ratio $Br(h_1^+ \to (\sum_i \nu_i)\mu^+)/Br(h_1^+ \to (\sum_i \nu_i)\tau^+)$ as function of O_{33}. For all curves, we have used the best fit point values for Δm_{23}^2, and the solar and

JHEP08(2006)036

atmospheric mixing angles. We have taken also $3 \times 10^{-6} < \kappa < 10^{-2}$ obtained when $0.2 < \mu < 500\,\mathrm{GeV}$, $M_1 = 200\,\mathrm{GeV}$ and $M_2 = 500\,\mathrm{GeV}$. The correlation regions correspond to the flat parts of the curves. The large O_{33} case determined by eq. (5.9) with $O_{12} = 0$ corresponds to the solid line in the right part of the plot, while the large O_{33} case with $O_{13} = 0$ correspond to the dashed line. In the same way, the small O_{33} case described by eq. (5.15) with $f_{13} = 0$ corresponds to the dotted line in the left part of the plot, while the small O_{33} case with $f_{12} = 0$ correspond to the dotted–dashed line. The scatter plot was obtained by searching for all solutions compatible with neutrino data at 3σ level, and keeping $O_{22} = (m_\mu/m_\tau)\,O_{33}$.

In the large O_{33} case described by eq. (5.9), the correlation region for $f_{ij} \gg O_{ij}$ is excluded because the parameters f_{ij} are above the values consistent with FCNC constraints (see tables 1 and 2). For the other correlation region, for which $O_{ij} \gg f_{ij}$, we have

$$\frac{Br(h_1^+ \to (\sum_i \nu_i)\mu^+)}{Br(h_1^+ \to (\sum_i \nu_i)\tau^+)} \sim \left(\frac{m_\mu}{m_\tau}\right)^2 \qquad \text{for } O_{ij} \gg f_{ij}. \tag{6.12}$$

As shown by the solid line at the right of figure 6, the contribution of f_{ij} can increase the ratio of branchings ratios up to a factor of 10^7. In this way the decay $h_1^+ \to (\sum_i \nu_i)\mu^+$ may become observable in future colliders. The dark gray (green) points were selected from the full scatter plot by choosing $O_{12} < 10^{-6}$. They are well fitted by the solid line which represents the one-parameter solution with $O_{12} = 0$ as given in eq. (5.9).

In the small O_{33} case with $f_{13} = 0$, we have

$$\begin{aligned}
&\frac{Br(h_1^+ \to (\sum_i \nu_i)\mu^+)}{Br(h_1^+ \to (\sum_i \nu_i)\tau^+)} \\
&\approx \begin{cases} \dfrac{2\,\tan^2 2\theta_{12}\,\tan^2\theta_{23}}{2\,\tan^2 2\theta_{12} + (1+\tan\theta_{23})^2}\dfrac{m_\tau^2}{m_\mu^2} & \text{for } O_{ij} \gg f_{ij} \\ \dfrac{1 + 2\,\tan\theta_{23} + \left(1 + 8\,\tan^2 2\theta_{12}\right)\,\tan^2\theta_{23}}{8\,\tan^2 2\theta_{12}\,\tan^2\theta_{23}} & \text{for } O_{ij} \ll f_{ij} \end{cases} \\
&\sim \begin{cases} \tan^2\theta_{23}\left(\dfrac{m_\tau}{m_\mu}\right)^2 & \text{for } O_{ij} \gg f_{ij} \\ 1 & \text{for } O_{ij} \ll f_{ij}. \end{cases}
\end{aligned} \tag{6.13}$$

As shown in the left part of figure 6, in this case the ratio of branching ratios is larger than one, and therefore an inverted hierarchy for the leptonic decays of the lightest charged Higgs is obtained. In this way, in the small O_{33} case, the most important leptonic decay channel for the charged Higgs h_1^+ must be $h_1^+ \to (\sum_i \nu_i)\mu^+$ instead of $h_1^+ \to (\sum_i \nu_i)\tau^+$.

Figure 7 shows the correlation region for $O_{ij} \gg f_{ij}$ in the small O_{33} case. The curves correspond to the ratio $Br(h_1^+ \to (\sum_i \nu_i)\mu^+)/Br(h_1^+ \to (\sum_i \nu_i)\tau^+)$, normalized by $(m_\mu/m_\tau)^2$, as a function of the atmospheric mixing angle, as expected from eq. (6.13) for the best fit point value of $\tan 2\theta_{12}$ (solid line) and its 3σ limits (dashed lines). The parameters are fixed as in figure 6 and the spread of the points can be understood from the uncertainty in the solar mixing angle. In this region the charged Higss decay rate $\Gamma(h^+ \to (\sum_i \nu_i)\mu^+)$ can be larger than decay rate $\Gamma(h^+ \to (\sum_i \nu_i)\tau^+)$ up to a factor of $(m_\tau/m_\mu)^2 = 280$.

JHEP08(2006)036

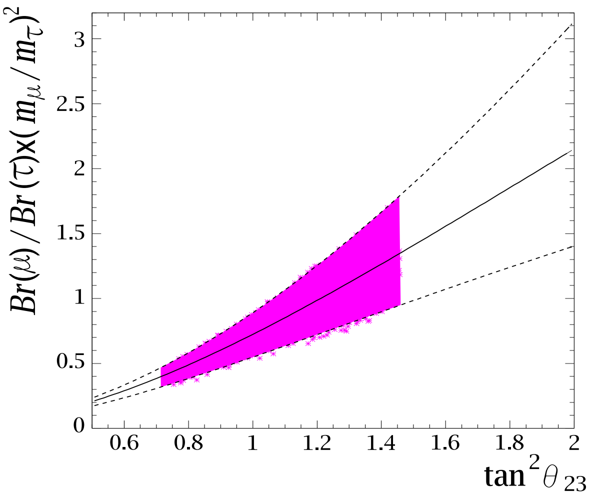

Figure 7: $Br(h_1^+ \to (\sum_i \nu_i)\mu^+)/Br(h_1^+ \to (\sum_i \nu_i)\tau^+)(m_\mu/m_\tau)^2$ as a function of $\tan\theta_{23}$ in the correlation region $O_{ij} \gg f_{ij}$ of the small O_{33} case. The solid curve corresponds to the best fit point value of $\tan 2\theta_{12}$, while the upper and lower curves corresponds to its 3σ limits. See text.

From figure 6 it can be seen that the large O_{33} region is divided in three sub-regions, region I where $10^{-3} \lesssim Br(h_1^+ \to (\sum_i \nu_i)\mu^+)/Br(h_1^+ \to (\sum_i \nu_i)\tau^+) \lesssim 1$, region II for which $1 \lesssim Br(h_1^+ \to (\sum_i \nu_i)\mu^+)/Br(h_1^+ \to (\sum_i \nu_i)\tau^+) \lesssim 10^2$ and region III characterised by $10^2 \lesssim Br(h_1^+ \to (\sum_i \nu_i)\mu^+)/Br(h_1^+ \to (\sum_i \nu_i)\tau^+) \lesssim 10^4$. Measurements of the ratio $Br(h_1^+ \to (\sum_i \nu_i)\mu^+)/Br(h_1^+ \to (\sum_i \nu_i)\tau^+)$ are sufficient to decide whether region I or III are realized. In region III there is an ambiguity that cannot be removed by measurements of the ratio $Br(h_1^+ \to (\sum_i \nu_i)\mu^+)/Br(h_1^+ \to (\sum_i \nu_i)\tau^+)$. However, in the small mixing limit the ambiguity can be removed. Recalling that in the small O_{33} region $f_{12} = 0$ or $f_{13} = 0$ one should expect, if this region is realized,

$$Br_s^\mu = Br_s^e + Br_s^\tau \quad \text{or} \quad Br_s^\tau = Br_s^e + Br_s^\mu. \tag{6.14}$$

Any deviation from these relations would exclude this region and in addition with a measurement of the type $1 \lesssim Br(h_d^+ \to (\sum_i \nu_i)\mu^+)/Br(h_d^+ \to (\sum_i \nu_i)\tau^+) \lesssim 10^2$ will indicate that region II is realized.

The curves in figure 6 are basically independent of the value of μ. However, along each curve, smaller values of O_{33} are excluded as μ decreases. On the other hand they depend on the specific value of M_1 and M_2. In fact, as the mixing angle $\sin 2\varphi$ increases the curves are shifted to the right. This is illustrated in figure 8 for the small O_{33} case with $f_{12} = 0$. All the remaining parameters are chosen as in figure 6. In particular the dotted line is the same as the one in figure 6.

In summary for the one parameter-solutions we have

$$\left(\frac{m_\mu}{m_\tau}\right)^2 \lesssim \frac{Br(h_1^+ \to (\sum_i \nu_i)\mu^+)}{Br(h_1^+ \to (\sum_i \nu_i)\tau^+)} \lesssim 10^4 \tag{6.15}$$

We have checked that this result holds for all the parameter space of the NMZM. For the large O_{33} region the decay rate $\Gamma(h_1^+ \to (\sum_i \nu_i)\mu^+)$ can be dominant if the f_{ij} Yukawa

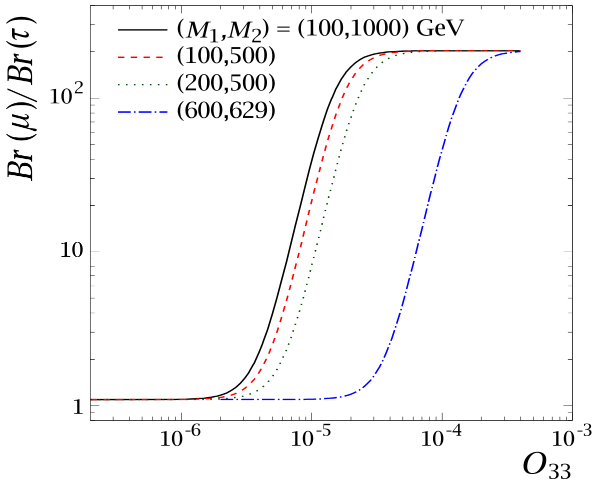

Figure 8: $Br(h_1^+ \to (\sum_i \nu_i)\mu^+)/Br(h_1^+ \to (\sum_i \nu_i)\tau^+)$ as a function of O_{33} and several pairs of M_1 and M_2 with $\mu = 100\,\mathrm{GeV}$. From left to right the curves have $\sin 2\varphi = 0.04$, 0.15, 0.17 and 0.99. The dotted line is the same that the curve in the left part of figure 6. See text.

couplings are sufficiently large. This mean that the usual hierarchy of the charged Higgs decays turns out to be different due to the new physics beyond the 2HDM, namely the new couplings involving the charged $\mathrm{SU}(2)_L$ singlet, $h^{\pm}$. On the other hand, for the small O_{33} region the decay rate $\Gamma(h_1^+ \to (\sum_i \nu_i)\mu^+)$ is dominant because of the rich structure of the general 2HDM, where, with some fine-tuning justified by neutrino physics, the couplings O_{ij} do not follow the hierarchy of the charged lepton mass matrix.

7. Conclusions

We have considered the version of the Zee model where both Higgs doublets couple to leptons. Instead of working with all the parameters we have focused on a model with minimal number of couplings consistent with neutrino physics data. We have shown that in the small mixing limit ($\varphi \ll 1$) certain ratios of branching ratios can be used to obtain information about the parameters of the model. Besides the charged Higgs leptonic decays we have also considered the decay $h_2^+ \to h_1^+ h^0$. We have found that this decay, if kinematically allowed, can be used to determine the value of the μ parameter. Moreover, measurements of $\Gamma(h_2^+ \to h_1^+ h^0)$ allow to decide whether the small mixing limit is realized or not.

Assuming that there are no large hierarchies among the couplings O_{i1} ($i = 1, 2, 3$) and O_{ij}, and using neutrino physics constraints we have shown that in this scheme only three parameters are independent. We have found that there are four regions, in this three-dimensional parameter space, determined by only O_{33}. We have shown that two of these four regions are governed by large values of O_{33} ($10^{-4} - 10^{-2}$) while the other two regions are governed by small values of O_{33} ($10^{-7} - 10^{-4}$).

We have analysed charged Higgs leptonic decays in the large as well as in the small O_{33} regimes and we have found: (i) in the large O_{33} case, there is a region in which the decays $h_1^+ \to \nu_i\mu^+$ and $h_1^+ \to \nu_i\tau^+$ are governed by the correponding Yukawas as in the 2HDM of type-I and type-II and another region where the decay $h_1^+ \to \nu_i \mu^+$ is enhanced and moreover can be larger than the decay to $h_1^+ \to \nu_i \tau^+$. (ii) In the small O_{33} case the decay $h_1^+ \to \nu_i \mu^+$ is always enhanced and is larger than the decay $h_1^+ \to \nu_i \tau^+$. Therefore we suggest that in order to test the model the decays of the charged Higgs to $\nu_i \mu^+$ should be searched along with the decays to $\nu_i \tau^+$. In fact, measurements of the ratio of branching ratios $Br(h_1^+ \to (\sum_i \nu_i)\mu^+)/Br(h_1^+ \to (\sum_i \nu_i)\tau^+)$ could give information about what region of this parameter space is realized.

At future colliders the decay channel $\nu\tau^+$ is very important for the discovery of charged Higgs bosons [27, 28]. For the LHC and SUSY like 2HDM, it has been claimed that the existence of a relatively heavy charged Higgs bosons, of mass up to 1 TeV, can be probed using the signal $h_1^+ \to \nu\tau^+$ [27]. At future linear colliders a single produced charged Higgs should be associated with the tau and the neutrino coming from the virtual charged Higgs decay [28]. According to our results, and illustrated by figure 6, the charged Higgs could emerge from a signal with $\nu_i \mu^+$ instead of $\nu_i \tau^+$. Moreover, for a light charged scalar $(M_1 < m_t)$ the ratio of branching ratios, $Br(h_1^+ \to (\sum_i \nu_i)\mu^+)/Br(h_1^+ \to (\sum_i \nu_i)\tau^+)$ should be measurable.

Acknowledgments

We thank W. Porod and E. Nardi for very useful suggestions. Especially to M. Hirsch for his advice as well as for critical readings of the manuscript. D.A. wants to thanks the *"Instituto de Física de la Universidad de Antioquia"* for their hospitality. This work was supported by Spanish grants BFM2002-00345 and FPA2005-01269. D.A. is supported by a Spanish PhD fellowship by M.C.Y.T. D.R. was partially supported by **ALFA-EC** funds.[5]

A. The Three-parameter solution

From the set of eqs. (5.7) we choose to express f_{12}, f_{13}, f_{23} and O_{13} in terms of O_{33}, O_{22}, and O_{12}

$$f_{12} = -\frac{A}{B}\frac{m_\tau\sqrt{\Delta m^2_{23}}}{m_\mu m_\tau}\frac{1}{O_{33}} \tag{A.1}$$

$$f_{13} = \left[\frac{\frac{m_\mu}{m_\tau}\left(\frac{\sqrt{2}\,O_{22}}{O_{33}} + \frac{O_{12}\,(1+\tan\theta_{23})}{O_{33}\,\tan 2\theta_{12}\,\tan\theta_{23}}\right) - \sqrt{2}}{\kappa\,\left(1-\frac{m_\mu O_{22}}{m_\tau O_{33}}\right)\left(1+\frac{1}{\tan\theta_{23}}\right)}\right]\frac{\sqrt{\Delta m^2_{23}}}{m_\tau}\frac{1}{O_{33}} \tag{A.2}$$

$$f_{23} = \frac{1}{\kappa\,\left(1-\frac{m_\mu\,O_{22}}{m_\tau\,O_{33}}\right)\tan 2\theta_{12}}\frac{\sqrt{\Delta m^2_{23}}}{m_\tau}\frac{1}{O_{33}} \tag{A.3}$$

$$O_{13} = \frac{2\sqrt{2}\,O_{12}\,\tan 2\theta_{12} - O_{22}\,(1+\tan\theta_{23})}{2\,\left[\sqrt{2}\,O_{22}\,\tan 2\theta_{12}\,\tan\theta_{23} + O_{12}\,(1+\tan\theta_{23})\right]}O_{33} \tag{A.4}$$

[5] This document has been produced with the assistance of the European Union. The contents of this document is the sole responsibility of the authors and can in no way be taken to reflect the views of the European Union.

JHEP08(2006)036

where

$$A = \left[1 + \left(2 + 4\,\tan^2 2\theta_{12}\right)\,\tan\theta_{23} + \tan^2\theta_{23}\right] - 2\,\frac{m_\mu}{m_\tau}\,\tan 2\theta_{12}\,\left[2\,\frac{O_{22}}{O_{33}}\,\tan 2\theta_{12}\,\tan\theta_{23} + \sqrt{2}\,\frac{O_{12}}{O_{33}}\,(1 + \tan\theta_{23})\right] \tag{A.5}$$

$$B = 2\,\kappa\,\left(\frac{m_\mu}{m_\tau}\frac{O_{22}}{O_{33}} - 1\right)\,\tan 2\theta_{12}\,(1 + \tan\theta_{23}) \times \left[\sqrt{2}\,\frac{O_{22}}{O_{33}}\,\tan 2\theta_{12}\,\tan\theta_{23} + \frac{O_{12}}{O_{33}}\,(1 + \tan\theta_{23})\right] \tag{A.6}$$

References

[1] KamLAND collaboration, K. Eguchi et al., *First results from KamLAND: evidence for reactor anti-neutrino disappearance*, *Phys. Rev. Lett.* **90** (2003) 021802 [hep-ex/0212021].

[2] Super-Kamiokande collaboration, S. Fukuda et al., *Solar B-8 and he p neutrino measurements from 1258 days of super-Kamiokande data*, *Phys. Rev. Lett.* **86** (2001) 5651 [hep-ex/0103032].

[3] M. Gell-Mann, P. Ramond and R. Slansky, *Complex spinors and unified theories*, in *Supergravity*, P. van Nieuwenhuizen & D.Z. Freedman eds., North Holland Publ. Co., 1979, Print-80-0576 (CERN);
T. Yanagida, in *KEK lectures*, O. Sawada and A. Sugamoto ed., KEK, 1979;
R.N. Mohapatra and G. Senjanovic, *Neutrino mass and spontaneous parity nonconservation*, *Phys. Rev. Lett.* **44** (1980) 912;
P. Minkowski, *$\mu \to e\gamma$ at a rate of one out of 1-billion muon decays?*, *Phys. Lett.* **B 67** (1977) 421.

[4] J. Schechter and J.W.F. Valle, *Neutrino masses in* $\mathrm{SU}(2) \times \mathrm{U}(1)$ *theories*, *Phys. Rev.* **D 22** (1980) 2227;
E. Ma and U. Sarkar, *Neutrino masses and leptogenesis with heavy Higgs triplets*, *Phys. Rev. Lett.* **80** (1998) 5716 [hep-ph/9802445].

[5] L.J. Hall and M. Suzuki, *Explicit R parity breaking in supersymmetric models*, *Nucl. Phys.* **B 231** (1984) 419;
G.G. Ross and J.W.F. Valle, *Supersymmetric models without R parity*, *Phys. Lett.* **B 151** (1985) 375;
J.R. Ellis, G. Gelmini, C. Jarlskog, G.G. Ross and J.W.F. Valle, *Phenomenology of supersymmetry with broken R parity*, *Phys. Lett.* **B 150** (1985) 142.

[6] M. Hirsch, M.A. Diaz, W. Porod, J.C. Romao and J.W.F. Valle, *Neutrino masses and mixings from supersymmetry with bilinear r-parity violation: a theory for solar and atmospheric neutrino oscillations*, *Phys. Rev.* **D 62** (2000) 113008 [hep-ph/0004115];
K. Choi, E.J. Chun and K. Hwang, *Lepton flavor violation and bilinear R-parity violation*, *Phys. Lett.* **B 488** (2000) 145 [hep-ph/0005262];
J.M. Mira, E. Nardi, D.A. Restrepo and J.W.F. Valle, *Bilinear R-parity violation and small neutrino masses: a self-consistent framework*, *Phys. Lett.* **B 492** (2000) 81 [hep-ph/0007266];
K.M. Cheung and O.C.W. Kong, *mu → e gamma from supersymmetry without R-parity*, *Phys. Rev.* **D 64** (2001) 095007 [hep-ph/0101347];
T.F. Feng and X.-Q. Li, *Neutrino oscillations in supersymmetry without lepton number conservation and R-parity*, *Phys. Rev.* **D 63** (2001) 073006 [hep-ph/0012300];

M. Hirsch, *R-parity violating supersymmetry and neutrino masses*, *Nucl. Phys.* **95** *(Proc. Suppl.)* (2001) 252;
E.J. Chun and S.K. Kang, *One-loop corrected neutrino masses and mixing in supersymmetric standard model without r-parity*, *Phys. Rev.* **D 61** (2000) 075012 [hep-ph/9909429];
E.J. Chun, D.-W. Jung and J.D. Park, *Bi-large neutrino mixing from bilinear R-parity violation with non-universality*, *Phys. Lett.* **B 557** (2003) 233 [hep-ph/0211310];
F. Borzumati and J.S. Lee, *Novel constraints on $\Delta_l = 1$ interactions from neutrino masses*, *Phys. Rev.* **D 66** (2002) 115012 [hep-ph/0207184];
E.J. Chun and J.S. Lee, *Implication of super-kamiokande data on R-parity violation*, *Phys. Rev.* **D 60** (1999) 075006 [hep-ph/9811201];
A. Abada, S. Davidson and M. Losada, *Neutrino masses and mixings in the MSSM with soft bilinear R_p violation*, *Phys. Rev.* **D 65** (2002) 075010 [hep-ph/0111332].

[7] D. Aristizabal Sierra, M. Hirsch, J.W.F. Valle and A. Villanova del Moral, *Reconstructing neutrino properties from collider experiments in a Higgs triplet neutrino mass model*, *Phys. Rev.* **D 68** (2003) 033006 [hep-ph/0304141].

[8] A. Zee, *A theory of lepton number violation, neutrino Majorana mass and oscillation*, *Phys. Lett.* **B 93** (1980) 389.

[9] K.S. Babu, *Model of 'calculable' Majorana neutrino masses*, *Phys. Lett.* **B 203** (1988) 132.

[10] L. Wolfenstein, *A theoretical pattern for neutrino oscillations*, *Nucl. Phys.* **B 175** (1980) 93.

[11] X.-G. He, *Is the Zee model neutrino mass matrix ruled out?*, *Eur. Phys. J.* **C 34** (2004) 371 [hep-ph/0307172].

[12] K.R.S. Balaji, W. Grimus and T. Schwetz, *The solar LMA neutrino oscillation solution in the Zee model*, *Phys. Lett.* **B 508** (2001) 301 [hep-ph/0104035].

[13] K. Hasegawa, C.S. Lim and K. Ogure, *Escape from washing out of baryon number in a two-zero- texture general Zee model compatible with the LMA-MSW solution*, *Phys. Rev.* **D 68** (2003) 053006 [hep-ph/0303252].

[14] M. Maltoni, T. Schwetz, M.A. Tortola and J.W.F. Valle, *Status of global fits to neutrino oscillations*, *New J.˜Phys.* **6** (2004) 122 [hep-ph/0405172].

[15] W.S. Hou, *Tree level $t \to ch$ or $h \to tanti - c$ decays*, *Phys. Lett.* **B 296** (1992) 179;
D. Chang, W.S. Hou and W.Y. Keung, *Two loop contributions of flavor changing neutral Higgs bosons to $\mu \to e\gamma$*, *Phys. Rev.* **D 48** (1993) 217 [hep-ph/9302267];
D. Atwood, L. Reina and A. Soni, *Phenomenology of two Higgs doublet models with flavor changing neutral currents*, *Phys. Rev.* **D 55** (1997) 3156 [hep-ph/9609279].

[16] S. Davidson and H.E. Haber, *Basis-independent methods for the two-Higgs-doublet model*, *Phys. Rev.* **D 72** (2005) 035004 [hep-ph/0504050].

[17] H.E. Haber and D. O'Neil, *Basis-independent methods for the two-Higgs-doublet model, II. The significance of* $\tan\beta$, *Phys. Rev.* **D 74** (2006) 015018 [hep-ph/0602242].

[18] ALEPH collaboration, A. Heister et al., *Search for charged Higgs bosons in e^+e^- collisions at energies up to $\sqrt{s} = 209\,gev$*, *Phys. Lett.* **B 543** (2002) 1 [hep-ex/0207054].

[19] OPAL collaboration, G. Abbiendi et al., *Two Higgs doublet model and model independent interpretation of neutral Higgs boson searches*, *Eur. Phys. J.* **C 18** (2001) 425 [hep-ex/0007040].

[20] DELPHI collaboration, J. Abdallah et al., *Searches for neutral Higgs bosons in extended models*, *Eur. Phys. J.* **C 38** (2004) 1 [hep-ex/0410017].

[21] M. Sher and Y. Yuan, *Rare b decays, rare tau decays and grand unification*, *Phys. Rev.* **D 44** (1991) 1461.

[22] J.A. Grifols and A. Mendez, *The WZH^{+-} coupling in* $\mathrm{SU}(2) \times \mathrm{U}(1)$ *gauge models*, *Phys. Rev.* **D 22** (1980) 1725.

[23] Particle Data Group collaboration, S. Eidelman et al., *Review of particle physics*, *Phys. Lett.* **B 592** (2004) 1.

[24] P.H. Frampton, S.L. Glashow and D. Marfatia, *Zeroes of the neutrino mass matrix*, *Phys. Lett.* **B 536** (2002) 79 [hep-ph/0201008].

[25] A. Barroso and P.M. Ferreira, *Charge breaking bounds in the Zee model*, *Phys. Rev.* **D 72** (2005) 075010 [hep-ph/0507128].

[26] S. Heinemeyer et al., *Toward high precision Higgs-boson measurements at the international linear e^+e^- collider*, *ECONF* **C0508141** (2005) ALCPG0214 [hep-ph/0511332].

[27] D.P. Roy, *Charged Higgs boson search at the LHC*, *AIP Conf. Proc.* **805** (2006) 110–116 [hep-ph/0510070]; *The hadronic tau decay signature of a heavy charged Higgs boson at LHC*, *Phys. Lett.* **B 459** (1999) 607 [hep-ph/9905542].

[28] S. Kanemura, S. Moretti and K. Odagiri, *Single charged Higgs boson production at next generation linear colliders*, *JHEP* **02** (2001) 011 [hep-ph/0012030].